

Centimetre continuum emission from young stellar objects in Cederblad 110

K. Lehtinen¹, J. Harju¹, S. Kontinen¹, and James L. Higdon²

¹ Observatory, Tähtitorninmäki, P.O. Box 14, 00014, University of Helsinki, Finland

² Department of Astronomy, 215 Space Sciences Building, Cornell University, Ithaca, NY 14853-6801, USA

Received / accepted

Abstract. The low-mass star formation region associated with the reflection nebula Cederblad 110 in the Chamaeleon I cloud was mapped with the Australian Telescope Compact Array (ATCA) at 6 and 3.5 cm. Altogether 11 sources were detected, three of which are previously known low mass young stellar objects associated with the nebula: the illuminating star IRS 2 (Class III, *Einstein* X-ray source CHX 7), the brightest far-infrared source IRS 4 (Class I), and the weak X-ray source CHX10a (Class III). The other young stellar objects in the region, including the Class 0 protostar candidate Cha-MMS1, were not detected. The radio spectral index of IRS 4 ($\alpha = 1.7 \pm 0.3$) is consistent with optically thick free-free emission arising from a dense ionized region, probably a jet-induced shock occurring in the circumstellar material. As the only Class I protostar with a 'thermal jet' IRS 4 is the strongest candidate for the central source of the molecular outflow found previously in the region. The emission from IRS 2 has a flat spectrum ($\alpha = 0.05 \pm 0.05$) but shows no sign of polarization, and therefore its origin is likely to be optically thin free-free emission either from ionized wind or a collimated jet. The strongest source detected in this survey is a new compact object with a steep negative spectral index (-1.1) and a weak linear polarization ($\sim 2\%$), which probably represents a background radio galaxy.

Key words. Stars: formation – ISM: individual objects: Cederblad 110 – ISM: clouds – Radio continuum: ISM

1. Introduction

The Cederblad 110 (Ced 110) reflection nebula in the Chamaeleon I molecular cloud is associated with one of the nearest low-mass star forming regions, with young stellar objects (YSOs) in all different phases from a pre-stellar clump and Class 0 protostellar candidate to a Class III pre-main sequence star (for YSO classification, see Lada (1987) and André et al. (1993)). The region is therefore favourable for studies of the dependence of radio continuum emission on the stellar evolutionary stage. On the other hand, a centimetre continuum mapping may reveal protostars, which have remained undetected in the infrared because of large optical depths. With these prospects as motivation we have mapped the central part of the nebula with the Australian Compact Array (ATCA) in continuum at 6 cm and 3.5 cm, in order to investigate the nature of the known stellar sources and to search for new protostellar candidates.

The region has been studied in great detail in the near-IR by Zinnecker et al. (1999) and Persi et al. (2001), in the mid-IR by Persi et al. (2000), and in the far-IR by Lehtinen et al. (2001). These papers contain all the relevant references to previous studies at various wavelengths ranging from 1.3 mm to X-rays. The YSOs identified in different surveys are listed in Table 1, which also gives the estimated infrared class, and the region of the electromagnetic spectrum where the source is de-

tected. The brightest star in visible light and in the X-rays is the weak-lined T Tauri star (Class III) IRS 2 (*Einstein* X-ray source CHX 7), which is the illuminating star of Ced 110. The Class I object IRS 4 is the most prominent far-infrared source, whereas the 1.3 mm continuum map is dominated by the Class 0 candidate Cha-MMS1 (the references are given in Table 1).

The distribution of molecular gas in the region has been studied by Mattila et al. (1989), and more recently by Mizuno et al. (1999). Mattila et al. (1989) detected a bipolar molecular outflow originating somewhere in the centre of Ced 110. Reipurth et al. (1996) mapped the centre of Ced 110 in continuum at 1.3 mm with a resolution of $22''$, and detected a marginally resolved bright dust continuum source they called Cha-MMS1. This source is coincident with the centre of a dense molecular clump studied in several molecular species by Kontinen et al. (2000). Reipurth et al. suggested that Cha-MMS1 contains a Class 0 protostar, which is the driving source of the molecular outflow and Herbig-Haro objects HH 49/50 located about $10'$ south of it. Since the central sources of Herbig-Haro flows are often detected in radio continuum (e.g. Rodríguez & Reipurth 1996), one of the aims of the observations discussed here was to verify - or invalidate - this suggestion.

In Sect. 2 of this paper we discuss briefly the mechanisms of radio emission associated with newly born stars. In Sect. 3 we describe our observational procedure. In Sect. 4 we present

the results and discuss the properties of individual sources in the light of previous surveys and some theoretical expectations. Finally, in Sect. 5 we summarize our conclusions.

2. Cm-wavelength continuum emission from YSOs

A large fraction of the youngest protostars, i.e. those belonging to the Classes 0 and I, have been detected in radio continuum at cm wavelengths (e.g. Anglada 1996; Rodríguez 1994). Class III objects are often associated with non-thermal radio emission. On the other hand, the detection rate amongst Class II protostars is lower than for the other classes. Gibb (1999) discussed this problem and suggested a scenario in which the dominant emission mechanism at cm wavelengths changes with the age of the YSO. According to this Class 0 and Class I objects, which are in the main and late accretion phase, respectively, emit thermal free-free emission from ionized jets, but this emission declines with time when the accretion rate or outflow efficiency (which are intimately linked) go down. Finally in the Class III stage, synchrotron emission from the exposed pre-main-sequence star becomes the dominant mechanism (see also Wilking et al. 2001).

Thermal emission can arise directly from stellar winds or collimated jets, or from shocks associated with jets or infall onto accretion disks. Non-thermal emission is related to magnetic fields close to the chromospherically active YSO, and/or to the star-disc interaction region. It is known that ionization by stellar photons is insufficient to produce the continuum emission in low luminosity sources such as those in Cederblad 110 (see e.g. Rodríguez et al. 1989). Reviews on possible thermal and non-thermal emission mechanisms in connection with young stars at different stages of evolution are given e.g. in Anglada (1996), André (1996), Panagia (1991), and Feigelson & Montmerle (1999). Models explaining the observed properties of the free-free emission sources are presented e.g. in Reynolds (1986, collimated ionized winds), Curiel et al. (1987, Herbig-Haro shocks), Neufeld & Hollenbach (1996, accretion shocks), and Ghavamian & Hartigan (1998, shocks in dense gas).

3. Observations and data reduction

Cederblad 110 was observed with the Australia Telescope Compact Array (ATCA), located at Narrabri, New South Wales, Australia. The observations were made on 2000 May 24 and 28, with the 1.5A array configuration. The frequencies 4.80 GHz (6 cm) and 8.64 GHz (3.5 cm) were observed simultaneously. The correlator configuration used provided at each frequency a total bandwidth of 104 MHz recorded as a 13 channel spectrum.

The calibration sources were selected from the ATCA Calibrator Source Catalogue (Reynolds 1997). The Seyfert 2 galaxy PKS 1934–638 was used as the primary flux calibrator, and the phase-reference calibrator was the quasar PKS 1057–797. The flux densities and the degrees of polarization of 1057–797 were found to be higher than those given in ATCA catalogue (see Table 2).

Table 1. YSOs associated with Ced 110

IR Class	designation	other name	spectrum	references
Class 0 or earlier	Cha-MMS1		1.3 mm	c,f
Class I	IRS 4	ISO-ChaI 84	IR	b,e,f,g,h
	IRS 6	ISO-ChaI 92	IR, X-ray	b,d,e,f,g
	ISO-ChaI 86	NIR 98	IR	e,g,f
	NIR 89		NIR	g
Class II	ISO-ChaI 97	NIR 131	IR	e
	ISO-ChaI 101 ¹	NIR 141	IR, X-ray	d,e
	NIR 72		NIR	g
	NIR 84		NIR	g
Class III	IRS 2	CHX 7, ISO-ChaI 75	IR, X-ray	a,b,d,e,f
	CHX10a	ISO-ChaI 117	IR, X-ray	a

a Feigelson & Kriss (1989); b Prusti et al. (1991); c Reipurth et al. (1996); d Carkner et al. (1998); e Persi et al. (2000); f Lehtinen et al. (2001); g Persi et al. (2001); h Zinnecker et al. (1999)

¹ The infrared spectral index between 2.2 μ m and 14.3 μ m, defined as $\alpha_{IR} \equiv d \log(\lambda F_{\lambda}) / d \log(\lambda)$, is -0.2. This value is close to the border between Class I and II objects (-0.3)

Table 2. Observational parameters. The position angle is measured to East from North

Target source	Ced 110	
Phase centre	R.A. 11 ^h 06 ^m 39.1 ^s (J2000.0)	Dec. -77°22'58" (J2000.0)
Frequency	4.80 GHz	8.64 GHz
Bandwidth	104 (13 × 8) MHz	104 (13 × 8) MHz
Flux calibrator	PKS 1934–638	
	$S_{4.80\text{GHz}} = 5.83 \text{ Jy}$	$S_{8.64\text{GHz}} = 2.84 \text{ Jy}$
Phase calibrator	PKS 1057–797	
	$S_{4.80\text{GHz}} = 2.58 \text{ Jy}$	$S_{8.64\text{GHz}} = 2.44 \text{ Jy}$
	Linear polarization	
	6% (P.A. 80°)	7% (P.A. 83°)
Image processing	Naturally weighted	
Synthesized beam	6.4'' × 5.8''	4.0'' × 3.7''
Beam position angle	-48°	-58°
RMS noise level	34 $\mu\text{Jy beam}^{-1}$	35 $\mu\text{Jy beam}^{-1}$

The observations were made in two 12 hours runs, alternating between the target source (25 minutes) and the phase calibrator (5 minutes). During the first night the observations were interrupted by rain for an hour, but during the second night the weather was excellent.

The data were calibrated and cleaned with the Miriad package (Sault et al. 1995). The inversion was performed using all the channel information (i.e. multifrequency synthesis). The flux densities of the detected sources were derived from

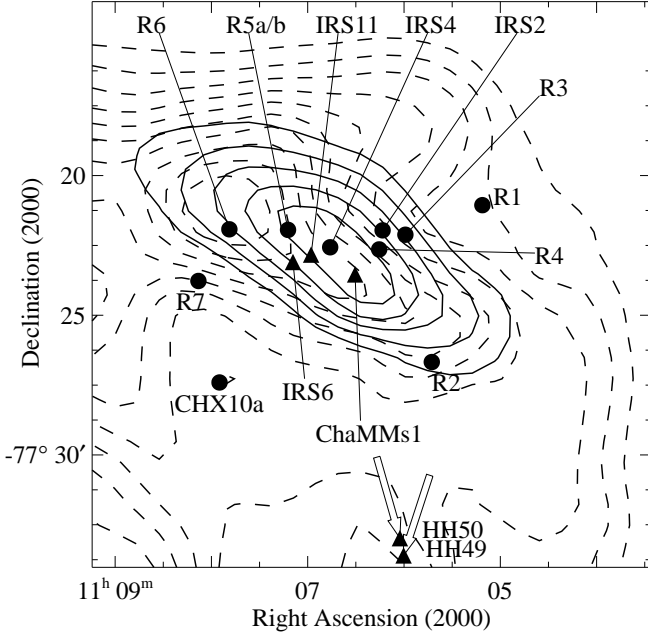


Fig. 1. Radio and infrared sources in the Cederblad 110. The cm continuum sources are marked with filled circles and the sources detected in other surveys are marked with filled triangles. Solid contours show the intensity of the $200\,\mu\text{m}$ emission ridge (Lehtinen et al. 2001), from 40 to 115 in steps of $15\,\text{MJy sr}^{-1}$. The dashed contours show the integrated intensity of $\text{C}^{18}\text{O}(J=1-0)$, from 0.2 to 2.0 in steps of $0.2\,\text{K km s}^{-1}$. The velocity vectors of Herbig-Haro 49 and 50 (mean of HH 50a-e) are indicated with arrows

naturally weighted images corrected for the primary beam responses. The noise levels at the centres of the images, and the synthesized beams are given in Table 2. Intensity maxima exceeding $3\times$ the local rms are considered as detections.

4. Results and discussion

Altogether 11 radio sources were identified by inspecting the maps visually. The characteristics of the detected sources are summarized in Table 3. In this table we give for each source the designation, the equatorial coordinates, the angular size, the flux densities at 3.5 and 6 cm and the spectral index, α , determined from the latter two values. The radio source Ced 110 R5 has two maxima, which are treated as separate components. The error in the α is estimated on the basis of random noise only. Objects that may be associated with the radio sources at other wavelengths were searched in the SIMBAD database.

Three of the detected sources are previously known objects: the infrared sources IRS 2 and IRS 4, and the X-ray source CHX10a. The rest are new sources, and we designate them as Ced 110 R1, Ced 110 R2, etc., where “Ced 110 R” stands for “Ced 110 radio source”. The mm-wave continuum source ChaMMs1 was not detected. As can be seen from Table 3, only three sources, Ced 110 R1, IRS 2 and IRS 4, are visible at both 3.5 and 6 cm.

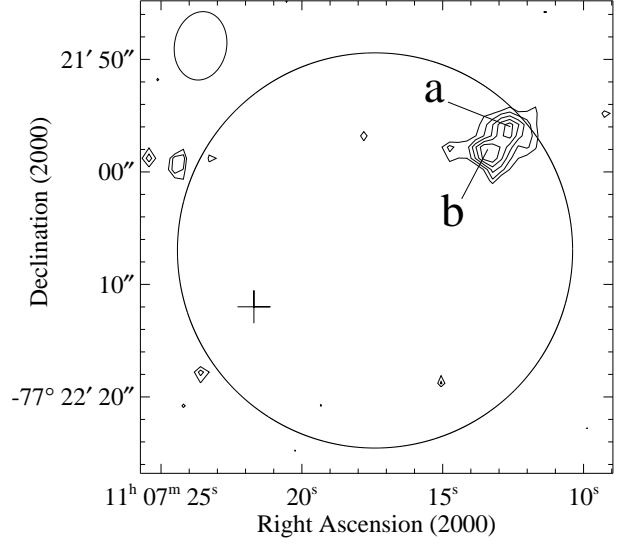


Fig. 2. The 6 cm contour map of the source Ced 110 R5. The contours are from $70\,\mu\text{Jy beam}^{-1}$ to $150\,\mu\text{Jy beam}^{-1}$ in steps of $20\,\mu\text{Jy beam}^{-1}$. The position of the infrared source ISO-ChaI 101 (the cross) and a circle depicting the X-ray intensity contour of 25 counts per pixel measured with ROSAT PSPC (Carkner et al. 1998) are shown. The FWHM beam size is shown at top left

The positions and sizes of the detected sources have been determined by two-dimensional gaussian fits. If a source is pointlike, the flux and its error given in Table 3 are the peak flux and its error of the gaussian fit. For resolved sources the flux is determined by adding up the pixels with flux density greater than the local 3σ rms noise value. The error of the integrated flux density for resolved sources is derived using the formula

$$\sigma = \sigma_0(N/\theta)^{1/2}, \quad (1)$$

where σ_0 is the rms noise in the background, N is the number of pixels over which the source is summed up, and θ is the number of pixels per beam.

If a source is detected at one frequency only and is found to be extended, the upper limit of integrated flux at the other frequency is estimated according to the formulation of Bertlan et al. (2001). We use the equation $S_{\text{lim}} = 3\sigma A^{0.7}$, where A is the source size in units of beam area, σ is the local rms noise, and assume a nominal 3σ detection as for point sources.

The locations of the radio sources are indicated with filled circles on the map presented in Fig. 1. This figure shows the extended far-IR emission ridge from Lehtinen et al. (2001) overlaid on an unpublished $\text{C}^{18}\text{O}(J = 1 - 0)$ integrated intensity map. The sources detected previously in other surveys are indicated with filled triangles.

In the following we first discuss spectral indices predicted by different models of thermal radio emission from YSOs, and then in the next subsection, the nature of individual sources

Table 3. Radio continuum sources detected in Cederblad 110. Flux upper-limits are calculated assuming a point source with a peak intensity of three times the rms. The positional accuracy is expected to be better than $2''$. The angular size is the measured FWHM along the major and minor axes at 3.5 cm, or at 6 cm if 3.5 cm data are not available, with uncertainty in parentheses. The quantity S is the intensity integrated over the source. The errors in S and α are estimated on the basis of the local rms noise.

Source	Position		Angular size [$''$]	S (3.5 cm) [mJy]	S (6 cm) [mJy]	α	Notes
	α (2000)	δ (2000)					
Ced 110 R1	11 ^h 05 ^m 13 ^s .9	-77°21'01".1	4.0×4.1 (0.1, 0.1)	7.8±0.1	14.74±0.02	-1.09±0.03	1
Ced 110 R2	11 ^h 05 ^m 44 ^s .5	-77°26'39".3	5.9×10.7 (0.1, 0.1)	< 1.3	1.6±0.1	< -0.3	2
Ced 110 R3	11 ^h 06 ^m 00 ^s .8	-77°22'05".9	3.1×4.2 (0.3, 0.4)	0.12±0.04	< 0.06	> 1.3	2
IRS 2	11 ^h 06 ^m 15 ^s .4	-77°21'56".8	3.6×3.9 (0.1, 0.1)	1.10±0.02	1.08±0.01	0.05±0.05	1
Ced 110 R4	11 ^h 06 ^m 17 ^s .4	-77°22'38".5	3.2×4.2 (0.6, 0.8)	0.04±0.02	< 0.03	> 0.1	2
IRS 4	11 ^h 06 ^m 46 ^s .5	-77°22'33".2	3.5×4.6 (0.3, 0.4)	0.17±0.02	0.06±0.01	1.7±0.3	1
Ced 110 R5a	11 ^h 07 ^m 13 ^s .4	-77°21'57".9	5.4 (0.3)	< 0.12	0.21±0.02	< -0.9	1
Ced 110 R5b	11 ^h 07 ^m 12 ^s .2	-77°21'55".7	5.3 (0.4)	< 0.12	0.15±0.02	< -0.4	1
Ced 110 R6	11 ^h 07 ^m 49 ^s .5	-77°21'54".6	5.7×6.9 (0.3, 0.4)	< 0.22	0.15±0.04	< 0.7	2
CHX10a	11 ^h 07 ^m 55 ^s .7	-77°27'25".0	6.5×13.7 (0.3, 0.6)	-	0.45±0.11	-	2
Ced 110 R7	11 ^h 08 ^m 08 ^s .0	-77°23'47".1	6.0×8.9 (0.1, 0.1)	< 1.3	1.33±0.09	< 0.0	2

¹ Flux is the peak flux of a gaussian fit

² Flux is derived by summing up the pixels having flux greater than the local 3σ noise

detected in this survey on the basis of their radio properties and association with known objects.

4.1. Spectral indices of thermal sources

The predicted spectral index α ($S_\nu \propto \nu^\alpha$) of the so called standard spherical wind, i.e. a fully ionized, constant velocity and isotropic stellar wind, is 0.6 at centimetre wavelengths (e.g. Panagia & Felli 1975). Reynolds (1986) have modelled continuum emission from both collimated and accelerated spherical flows. According to these results the spectral index can increase above 0.6 for an accelerated flow, but a collimated ionized flow produces a flat spectrum with $\alpha < 0.6$. Rodríguez et al. (1993) have shown that the spectral index expected from an ionized jet is always greater than -0.1, irrespective the geometry and possible clumpiness.

Optically thick free-free emission can be detected from shocks occurring in very dense gas, as in the situations of accreting material falling onto a circumstellar disk or a jet penetrating into dense circumstellar material (Neufeld & Hollenbach 1996; Ghavamian & Hartigan 1998).

4.2. Radio emission from the young stars IRS 2, IRS 4 and CHX10a, and thermal sources possibly associated with Ced 110

IRS 2 is the second strongest 3.5 cm source in this survey, and the third strongest at 6 cm. The spectral index is 0.05 ± 0.05 , and the radio continuum luminosity at 3.5 cm $L_{3.5\text{cm}} = 0.025 \text{ mJy kpc}^2$. The luminosities are estimated using the distance 150 pc to Chamaeleon I (Knude & Høg 1998). As an evolved YSO IRS 2 is probably not associated with a thick accretion disk. The ionized winds or collimated jets emanating from this star are therefore likely to proceed freely, and according to models quoted in Sect. 2 the free-free emission should

show a flat spectrum as indeed is the case. Consider the model of Reynolds (1986) for an isothermal, constant-velocity, fully ionized flow with $w(r) \propto r^\epsilon$, where $w(r)$ is the half-width of the jet perpendicular to its axis and r is the distance from the central source. In this model the spectral index in the optically thick case depends on ϵ according to $\alpha = 1.3 - 0.7/\epsilon$. The spectral index observed towards IRS 2 would then correspond to the collimation exponent $\epsilon = 0.6$.

The powerful X-ray emission associated with IRS 2 implies, on the other hand, magnetic activity close to its surface. Magnetic loops or fast shocks caused by ejecta from the surface may be sources of non-thermal radio emission. The observed spectral index is in fact consistent with moderately optically thick synchrotron emission. These kind of activities are generally associated with detectable circular polarization. No polarized signal is, however, detected towards this source. Without further evidence for the synchrotron model we think the more likely alternative is that the radio spectrum is dominated by free-free emission from ionized jets.

IRS 4: The radio source is located about $2''$ to the northwest from the position of the highly reddened illuminating star of the bipolar reflection nebula discovered by Zinnecker et al. (1999) (see also Persi et al. 2001). Taking the positional inaccuracies into account, the radio source is almost certainly associated with this star. The spectral index, 1.7 ± 0.3 , indicates optically thick free-free emission, which according to the models of Neufeld & Hollenbach (1996) and Ghavamian & Hartigan (1998) signifies shocks in dense circumstellar material. The existence of a massive circumstellar disk or envelope around IRS 4 is evident from the near-IR images of Zinnecker et al. (1999) and Persi et al. (2001). Far-IR ISOPHOT observations of Lehtinen et al. (2001), where IRS 4 is by far the strongest source in the region, indicate a large circumstellar mass. According to the estimates of Persi et al. the mass of the central object is very low ($0.1 - 0.3 M_\odot$), which suggests

that powerful accretion shocks are less likely. Interaction between stellar jets and surrounding material are therefore the most plausible origin of the radio continuum emission for this object.

IRS 4 lies close to the centre of the molecular outflow detected in ^{12}CO by Mattila et al. (1989). As the only Class I object in this region provedly associated with thermal jets IRS 4 is probably the central source of the outflow.

CHX10a: Weak emission at 6-cm originates close to the X-ray source CHX10a, which is classified as a weak-line T Tauri star, i.e. a Class III object (Feigelson & Kriss 1989; Feigelson et al. 1993). In the latter study the source was designated as CHXR28 (CHXR is for “Chamaeleon I X-ray ROSAT”), and it is also known as the infrared source ISO-ChaI 117 (Persi et al. 2000). At 3.5 cm the source lies outside the field of view limited by the primary beam response, and unfortunately we cannot derive even the upper limit for the spectral index. Judging from the nature of star, the 6 cm emission is likely to be synchrotron emission originating from magnetic loops close to the stellar surface.

Ced 110 R3 and 4: These weak sources lying close to IRS 2 in the centre of Ced 110 are detected at 3.5 cm only. The lower limits of their spectral indices are consistent with thermal emission. We therefore consider it possible that these sources are associated with the Chamaeleon I cloud, perhaps representing shocks associated with jets emanating from one of the young stars in the region.

4.3. Non-detections

Cha-MMS1: A Class 0 object should, by definition, show indirect evidence for the presence of a central protostellar object in the form of cm-wavelength continuum emission or a molecular outflow. Since Cha-MMS1 was not detected in either frequency band, and the centre of the molecular outflow is not coincident with it, Cha-MMS1 does not seem to fulfil the criteria for a Class 0 protostar. Probably it represents an earlier stage where violent processes have not yet taken effect. The empirical relation of Harvey et al. (2002) between the 3.6 cm continuum flux $S_{3.6\text{ cm}}$ and bolometric luminosity L_{bol} for Class 0 and I protostellar sources gives an upper limit of $L_{\text{bol}} \lesssim 0.17 L_{\odot}$, when the 3σ upper limit for the 3.5 cm flux density is used. The bolometric luminosity $\sim 0.45 L_{\odot}$ derived from far-IR observations (Lehtinen et al. 2001) is higher than this upper limit, suggesting that the Harvey et al. relation is not valid for Cha-MMS1, which supports the idea that it does not belong to Class 0.

IRS 6: The Class I object IRS 6 belongs to the most luminous YSOs in the region along with IRS 2 and IRS 4. Persi et al. (2001) resolved this object into two components, IRS 6a and 6b, of which 6a dominates the mid-IR and far-IR emission. The far-IR and sub-mm data suggest that the negative result at cm wavelengths reflects profound differences between IRS 6 and IRS 4, and not merely temporal variability (e.g. Lucas et al. 2000). The far-IR spectrum of IRS 6 indicates much weaker circumstellar dust emission than in the case of IRS 4 (see Table 2

of Lehtinen et al. 2001). Moreover, as discussed in Carkner et al. (1998), the fact that (unlike IRS 4) it was not detected in the 1.3 mm survey of Henning et al. (1993) betokens a lack of circumstellar envelope, and perhaps a more advanced stage of protostellar evolution. The non-detection in the radio could then be understood in terms of the evolutionary scenario laid out by Gibb (1999), and summarized in Sect. 2.

4.4. Background objects

The deep optical and near-IR surveys performed towards Ced 110 (Persi et al. 2001) have probably revealed all Class III protostars in the region, for example the “naked YSO”-type objects with non-thermal radio spectra detected by André et al. (1992) in the ρ Ophiuchi cloud. Radio sources with negative spectral indices in our maps without any counterpart in the near-IR are therefore likely to be background objects, and as we are rather far from the Galactic plane, these objects are probably radio galaxies, although pulsars cannot be totally excluded.

Ced 110 R1: The previously unknown compact source Ced 110 R1 is by far the strongest 6 cm and 3.5 cm source in this survey. The rather large negative spectral index, $\alpha = -1.09 \pm 0.03$, can be found among the various classes of extragalactic steep-spectrum sources, but would not be unusual for pulsars, which often have, however, still steeper spectra in this wavelength range (see e.g. Kaplan et al. 2000). Ced 110 R1 can be detected also in the Stokes Q and U images (220 and $160 \mu\text{Jy}$, respectively), but not in Stokes V. As the I flux density is about 14.7 mJy , these results indicate linear polarization at the level 1.8%. Further observations to investigate the nature of this bright object seem warranted.

Ced 110 R5: This marginally resolved source detected at 6 cm is located within the dust emission ridge (see Fig. 1), close to the grouping of YSOs containing IRS 2, 4, 6 and 11. A contour image of Ced 110 R5 is presented in Fig. 2. The image shows two emission maxima (components a and b) separated by $\sim 3''$, and the southern source has an extension at about $2-3\sigma$ level reaching out to the east. The parameters of the components given in Table 3 were determined by fitting two gaussian functions to the image. Both sources have negative spectral indices. The object lies close to the X-ray source which Carkner et al. (1998) associated with the infrared source ISO-ChaI 101 (see their Fig. 1). The angular distance to Ced 110 R5 from centre of the X-ray source ($\sim 15''$) is about the same as from there to ISO-ChaI 101 (see Fig. 2). Judging from the positional coincidence the association of Ced 110 R5 with the X-ray source is equally likely as it is for ISO-ChaI 101. The separation between Ced 110 R5 and ISO-ChaI 101 (corresponding to 4000 AU at a distance of 150 pc) is too large to expect a connection. Therefore, as it is not associated with an infrared source, Ced 110 R5 is probably a background radio galaxy.

Ced 110 R2, Ced 110 R6 and Ced 110 R7: These sources are visible at 6 cm only and for R2 and R7 the upper limits of the spectral indices are negative, suggesting optically thin synchrotron emission. The large upper limit of the spectral

index of R6 is due to its location close to the outer edge of the map. Most likely these sources background radio galaxies. Ced 110 R2 and Ced 110 R7 are slightly extended with elliptical shapes. Ced 110 R2 is the second brightest source at 6 cm. It lies at a distance of about $10''$ from the X-ray source CHXR 15, which Feigelson et al. (1993) identified with a star visible on the ESO/SERC Sky Survey plates with an R-band magnitude of 16.0. The radio sources Ced 110 R6 and Ced 110 R7 have no counterpart in other surveys. The former object lies in the direction of the extended $200\mu\text{m}$ emission ridge, but the location is probably purely coincidental.

5. Conclusions

Three YSOs associated with the Cederblad 110 star formation region have been detected with the Australian Telescope Compact Array at 3.5 cm and 6 cm. These three sources, IRS 4 (Class I), IRS 2 (Class III) and CHX10a (Class III) represent different stages of stellar evolution. IRS 2 shows a flat spectrum but no polarization, and these properties can be explained by optically thin free-free emission from ionized stellar wind or a collimated jet. The spectral index of IRS 4 is consistent with optically thick free-free emission, probably arising from a jet-driven shock in the circumstellar material. The other luminous Class I source IRS 6 is not detected in radio, but there are indications in previous sub-mm and far-IR observations that it has less circumstellar material than IRS 4 and can thus represent a more evolved protostar. The fact that of the four Class I objects in the region only the strongest far-IR source (IRS 4) is detected in radio, suggests a correlation between the outflow activity and the amount of circumstellar matter. The radio properties of IRS 2 and IRS 4, and the quietness of IRS 6, conform with the concept that the radio activity and the nature of the emission change in the course of protostellar evolution, as discussed e.g. by Gibb (1999) and Feigelson & Montmerle (1999). The spectral index of radio emission from CHX10a could not be determined because it lies outside the FOV at 3.5 cm. As the star is a Class III object associated with X-ray emission, the 6 cm emission is probably non-thermal.

The Class 0 candidate ChaMMS-1 (Reipurth et al. 1996) is not detected in radio. Thus, since there is no clear evidence for jets or outflow associated with this source, we suggest that it represents a still earlier protostellar stage or a pre-stellar clump. As a Class I protostar with optically thick ionized wind IRS 4 is the most likely candidate for the central source of the molecular outflow detected by Mattila et al. (1989).

Eight radio sources with no counterpart in other wavelengths were detected in the region of Ced 110. Two of these additional sources were detected at 3.5 cm only and can be shocks associated with the star forming region. The rest have negative spectral indices and are probably radio galaxies. The brightest of these is a compact source with a spectral index of -1.1 and a weak linear polarization ($\sim 2\%$) at 6 cm. Further radio observations of this source seem warranted.

Acknowledgements. We wish to thank the ATCA staff for their help during our observations. We are grateful to Professor Kalevi Mattila for helpful comments on the manuscript. The work of K.L., S.K. and

J.H. has been supported by the Finnish Academy through grants Nos. 173 727 and 174854, which is gratefully acknowledged. The work of S.K. has been supported by the Väisälä Foundation of the Finnish Academy of Science and Letters. This research has made use of the SIMBAD database, operated at CDS, Strasbourg, France.

References

- André P., Deeney B.D., Phillips R.B. et al. 1992, *ApJ* 401, 667
- Andre P., Ward-Thompson D., & Barsony M. 1993, *ApJ* 406, 122
- André P. 1996, In *ASP Conf. Ser. 93, Radio Emission from the Stars and the Sun*, eds. A.R. Taylor & J.M. Paredes (San Francisco: ASP), 3
- Anglada G. 1996, In *ASP Conf. Ser. 93, Radio Emission from the Stars and the Sun*, eds. A.R. Taylor & J.M. Paredes (San Francisco: ASP), 3
- Beltrán M.T., Estalella R., Anglada G., & Rodríguez L.F. 2001, *AJ* 121, 1556
- Carkner L., Kozak J.A., & Feigelson E.D. 1998, *AJ* 116, 1933
- Curiel S., Cantó J., & Rodríguez L.F. 1987, *Rev. Mex. Astron. Astrofis.* 14, 595
- Feigelson E.D., & Kriss G.A. 1989, *ApJ* 338, 262
- Feigelson E.D., & Montmerle T. 1999, *ARA&A*, 37, 363
- Feigelson E.D., Casanova S., Montmerle T. et al. 1993, *ApJ* 416, 623
- Gibb A.G. 1999, *MNRAS* 304, 1
- Ghavamian P., & Hartigan P. 1998, *ApJ* 501, 687
- Harvey D.W.A., Wilner D.J., Francesco J.D. et al. 2002, *AJ* 123, 3325
- Henning T., Pfau W., Zinnecker H., & Prusti T. 1993, *A&A* 276, 129
- Kaplan D.L., Cordes J.M., Condon J.J., & Djorgovski S.G. 2000, *ApJ* 529, 859
- Knude J., Høg, E. 1998, *A&A* 338, 897
- Kontinen S., Harju J., Heikkilä A., & Haikala L.K. 2000, *A&A* 361, 704
- Lada, C. J. 1987, *IAU Symp. 115: Star Forming Regions*, 115, 1
- Lehtinen K., Haikala L.K., Mattila K., & Lemke D. 2001, *A&A* 367, 311
- Lucas P.W., Blundell K.M., & Roche P.F. 2000, *MNRAS* 318, 526
- Mattila K., Liljeström T., & Toriseva M. 1989, in *Low Mass Star Formation and Pre-Main Sequence Objects*, Reipurth B. (ed.), *ESO Conference and Workshop Proceedings* 33, p. 153
- Neufeld D.A., & Hollenbach D.J. 1996, *ApJ* 471, L45
- Panagia N. 1991, in *The physics of star formation and early stellar evolution*, Kluwer Academic Publishers, eds. Lada C.J., Kylafis N.D.
- Panagia N., & Felli M. 1975, *A&A* 39, 1
- Persi P., Marenzi A.R., & Olosson G. 2000, *A&A* 357, 219
- Persi P., Marenzi A.R., Gómez M., & Olofsson G. 2001, *A&A* 376, 907
- Prusti T., Clark F.O., Whittet D.C.B., Laurejs R.J., & Zhang C.Y. 1991, *MNRAS* 251, 303
- Reipurth B., Nyman L.-Å., & Chini R. 1996, *A&A* 314, 258
- Reynolds S.P. 1986, *ApJ* 304, 713
- Reynolds J.E. 1997, *ATCA Calibrator Source Catalogue*. <ftp://ftp.atnf.csiro.au/pub/atnfdocs/guides/at.cat>
- Rodríguez L.F. 1994, *Rev. Mex. Astron. Astrofis.* 29, 69
- Rodríguez L.F. 1997, in *Herbig-Haro Flows and the Birth of Low Mass Stars*, eds. Reipurth B. & Bertout C., *IAU Symposium* No. 182, p. 83
- Rodríguez L.F., Myers P.C., Cruz-González I., & Terebey S. 1989, *ApJ* 347, 461
- Rodríguez L.F., Martí J., Cantó J. et al. 1993, *Rev. Mex. Astron. Astrofis.* 25, 23

- Rodríguez L.F., & Reipurth B. 1996, *Rev. Mex. Astron. Astrofis.* 32, 27
- Sault R.J., Teuben P.J., Wright M.C.H. 1995, in Shaw R., Payne H.E., Hayes J.J.E., eds, *Astronomical Data Analysis Software and Systems IV*, ASP Conf. Ser., Vol. 77. Astron. Soc. Pac., San Francisco, p. 433
- Wiling B.A., Bontemps S., Schuler R.E. et al. 2001, *ApJ* 551, 357
- Zinnecker H., Krabbe A., McCaughrean M.J. et al. 1999, *A&A* 352, L73